

Grafted natural rubber-based polymer electrolytes: ATR-FTIR and conductivity studies

A. M. M. Ali · R. H. Y. Subban · H. Bahron · T. Winie ·
F. Latif · M. Z. A. Yahya

Received: 4 October 2007 / Revised: 7 December 2007 / Accepted: 14 December 2007 / Published online: 14 January 2008
© Springer-Verlag 2007

Abstract Attenuated total reflectance–Fourier transformed infrared spectroscopy measurement is employed to study the interactions between the components of 30% methyl-grafted natural rubber (MG30), lithium trifluoromethanesulfonate (LiCF₃SO₃ or LiTF), and propylene carbonate (PC). Vibrational spectra data of LiTF reveals that the $\nu_s(\text{SO}_3)$ at 1,045 cm⁻¹, $\delta_s(\text{CF}_3)$ at 777 cm⁻¹, and C=O stretching mode at 1,728 cm⁻¹ for MG30 have shifted to lower wave numbers in MG30–LiTF complexes indicating that complexation has occurred between MG30 and LiTF. The solvation of lithium ion is manifested in Li⁺ ← O=C interaction as shown by the downshifting and upshifting of C=O mode at 1,788 to 1,775 cm⁻¹ and $\nu_{as}(\text{SO}_3)$ at 1,250 to 1258 cm⁻¹, respectively, in LiTF–PC electrolytes. There is no experimental evidence of the interaction between MG30 and PC. Competition between MG30 and PC on associating with lithium ion is studied, and the studies show that the interaction between MG30–LiTF is stronger than that of the PC–LiTF in plasticized polymer–salt complexes. The effect of PC on the ionic conductivity of the MG30–LiTF system is explained in terms of the polymer, plasticizer, and salt interactions. The temperature dependence of conductivity of the polymer films obeys the Vogel–Tamman–Fulcher relation. Values of conductivity and activation energy of the MG30-based polymer electrolyte systems are presented and discussed.

Keywords Natural rubber · MG30 · Infrared spectroscopy · Conductivity

Introduction

The study of polymer electrolytes was initiated by Fenton et al. [1] in 1973, but their technological significance was only appreciated later after the publications by Armand et al. [2, 3]. To date, several types of polymer electrolytes such as poly(ethylene oxide) (PEO), poly(acrylonitrile), poly(methyl methacrylate) (PMMA), poly(vinyl chloride), and poly(vinylidene fluoride) have been developed and characterized. These have been prepared and characterized as solid polymer electrolytes (SPEs) and gelled polymer electrolytes (GPEs) systems. SPEs are lightweight and show good thin film-forming ability, processing ease, flexibility, and elasticity, but they suffer low ionic conductivity at room temperature [4]. GPEs seem to be an attractive alternative to SPEs as they possess higher ambient ionic conductivities ($\sim 10^{-3}$ S cm⁻¹) and good dimensional stability [5, 6]. The major drawbacks of GPEs are their insufficient strength to be used as electrode separators and their creep under pressure.

Grafted polymers have been reported to have an ability to improve the mechanical properties of GPEs, increase adhesion to the electrode, increase solvent intake, change solubility characteristics, and enhance conductivity [7–9]. Nasef and Saidi [10] explored the effect of adding grafted styrene onto poly(vinylidene fluoride) and found it to be a successful method in increasing the ionic conductivity and reducing the inherent crystallinity of the host polymer. Idris and Glasse [11, 12] has explored the potential application of epoxy natural rubber, ENR25, and PMMA-grafted ENR50 as an electrolyte for lithium ion battery, but their conductivity is far from adequate for practical room temperature applications.

A. M. M. Ali · R. H. Y. Subban · H. Bahron · T. Winie · F. Latif ·
M. Z. A. Yahya (✉)
Ionic Materials and Devices Research Laboratory,
Centre of Advanced Materials, Institute of Science,
Universiti Teknologi MARA,
40450 Shah Alam, Malaysia
e-mail: mzayahya@yahoo.com

A. M. M. Ali
e-mail: ammali9897@yahoo.co.uk

The low ionic conductivity is caused by the low mobility of the charge carriers in the polymer matrix, and the main factor that limits the ionic mobility is ion aggregation or ion association in polymer electrolytes [13]. This effect reduces the efficiency of the electrolytes for any potential electrochemical usage.

One of the methods to improve the conductivity of a polymer electrolyte is by adding a plasticizer, which has been shown to significantly increase the ionic conductivity [14]. The effect of plasticizers generally is to reduce the glass transition temperature of the polymer, which helps to increase the segmental motion of the polymer backbone hence producing free volume [13, 15]. The existence of the free volume enables ions to migrate easily through the void. The high dielectric constant and low viscosity of plasticizers enable them to be incorporated with the polymer host to facilitate the formation of dissociated ions [16]. Southall et al. [17] investigated the correlation between ionic conductivity and low viscosity of plasticizers, leading to high ionic mobility and hence conductivity. Many plasticizer–polymer–salt interactions have been studied [18–21]. The interaction between ions, plasticizers, and polymers could be investigated using Raman and infrared spectroscopy, and some qualitative measurements have been reported [22]. Ion-pairing effects have also been reported in which a weak interaction of the anions with the dipoles causes the functional group of the polymer to interact with the cation [22]. The use of propylene carbonate (PC) or ethylene carbonate as plasticizers on PEO–lithium trifluoromethanesulfonate (LiTF) has been shown to reduce ion association and increase the amorphous nature of polymer–salt complexes via preferential interaction with the crystalline PEO phase [23, 24].

In the present work, gel electrolytes made up of LiTF and 30% methyl-grafted natural rubber (MG30) in the presence of PC as a plasticizer are cast using tetrahydrofuran (THF) as a solvent. Attenuated total reflectance (ATR)–Fourier transformed infrared spectroscopy (FTIR) studies are conducted on the gelatinized MG30 added with varying percentage of salt (5–50%), polymer (5–50%), and plasticizer (23–61%). ATR-FTIR spectroscopy is used to observe the interactions between the various components because of variation in compositions and percentages of plasticizer–salt, polymer–salt, and plasticized polymer–salt in the mixture to predict the occurrence of chemical interactions. Functional groups in the components absorb the infrared radiation and produce characteristic vibrations. The absorption wavelength depends on the relative mass of the functional group, the force constant of the bonds, and the geometry of the atoms. In this paper, ATR-FTIR is used to establish the interactions between MG30–LiTF, LiTF–PC, and MG30–LiTF–PC. Such interactions could be assigned by studying their vibrational modes characteristic of

relevant functional groups. The conductivity of MG30–LiTF–PC systems are then correlated to the various interaction observed in ATR-FTIR spectroscopy.

Experimental

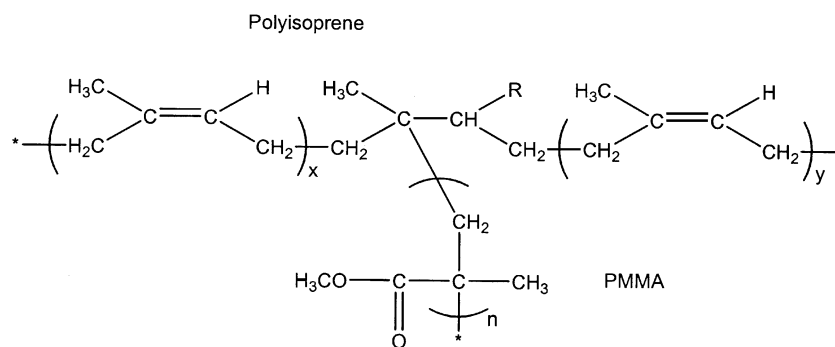
MG30 was obtained commercially and used as purchased. LiTF obtained from Aldrich was predried for more than 48 h under vacuum at 110 °C. PC from Aldrich was distilled over molecular sieve type 4A before use. All samples were prepared using the solution cast technique. One gram each of MG30 was dissolved in 25 ml THF for about 48 h. A different stoichiometric ratio of LiTF was dissolved in a different solution of host polymer in a closed Scott bottle and continuously stirred for several hours at room temperature. The solutions were casted into glass Petri dishes, and the films were dried in a vacuum oven at 60 °C for 48 h before conductivity testing. The composition with the highest conducting sample was used in preparing the plasticized samples. The PC with different stoichiometric ratio was added on each section, and the same procedure was employed. All resulting samples were kept in an argon-filled MBRAUN glove box ($O_2 < 0.1$ ppm; $H_2O < 0.1$ ppm) to ensure the films completely free from the moisture. ATR-FTIR spectra were recorded using the Perkin Elmer Spectrum-One spectrometer in the frequency range 650 to 4,000 cm^{-1} with a resolution of 2 cm^{-1} . The samples were placed on the horizontal face of the internal reflectance crystal of Zinc Selenide (ZnSe) where total internal reflection occurred along the crystal–sample interface. The impedance spectroscopy of all samples were performed using Hioki 3532-50 LCR HiTESTER in the frequency range of 100 Hz to 1 MHz over the temperature range of 303–383 K. Samples were mounted on the conductivity holder with stainless steel (SUS316) electrodes.

Results and discussion

ATR-FTIR spectroscopy of pure polymer (MG30)

MG30 has a chemical structure as illustrated in Fig. 1, and Fig. 2 shows the ATR-FTIR spectrum of pure MG30. The characteristic peaks of the saturated aliphatic sp^3 C–H bonds are observed at 2,962, 2,923, and 2,853 cm^{-1} which are assigned to ν_{as} (CH_3), ν_{as} (CH_2), and ν_s (CH_2), respectively. In the region of 1,900–2,800 cm^{-1} , no absorption frequencies are observed except for a weak band at 2,726 cm^{-1} , which is also due to the C–H stretching mode [25]. Other fundamental vibrational frequencies observed in MG30 can be assigned to the functional groups found in natural rubber (polyisoprene) and PMMA. A

Fig. 1 Chemical structure of MG30 (in the structure: R is a free radical)



strong and sharp peak located at $1,728\text{ cm}^{-1}$ is attributed to the symmetric stretching mode of $\text{C}=\text{O}$ in pure MG30. This is consistent with the observations reported by Kumutha and Alias [26]. The $\text{C}=\text{C}$ stretching, CH_3 symmetric deformation, and CH_2 -twisting modes of polyisoprene observed at $1,662$, $1,375$, and $1,239\text{ cm}^{-1}$, respectively, also appear in the spectrum of MG30. These bands are in good agreement with the results reported by Arjunan et al. [27]. Other characteristic peaks of PMMA and polyisoprene could also be found in the infrared spectrum of the MG30 polymer. The detailed assignments of the peaks observed from the MG30 spectrum are listed in Table 1.

Polymer–salt interactions

The characteristic bands of saturated polymeric ester group of methyl methacrylate are of major interest in the detection of ionic interactions. The oxygen atom at the $\text{C}=\text{O}$ and $\text{C}-\text{O}$ functional groups carries lone pairs of electrons, which are donated to Li^+ in forming complexes with the lithium salt. Figure 3 shows the comparative infrared spectra of LiTF,

MG30, MG30 with 35 wt% LiTF, and MG30 with 45 wt% LiTF. The vibrational frequencies of several functional groups of the triflate ion can be used to investigate the nature of ionic dissociations and interactions in MG30–LiTF complexes. Figure 3a(i) shows a peak at $1,045\text{ cm}^{-1}$ assignable to the $\nu_s(\text{SO}_3)$ (symmetric stretching mode of SO_3) [22], which has shifted to a lower wave number at $1,039\text{ cm}^{-1}$ with a reduced intensity in the presence of MG30 as can be seen in Fig. 3a(iii). A further shifting of this peak to $1,035\text{ cm}^{-1}$ is also noticeable with increasing salt concentration as shown in Fig. 3a(iv). The shifting of this peak to form a broad band could be related to the number of monodenate ion pairs [19, 22] present in the MG30–LiTF complexes, and it is strongly believed that this may affect the conductivity of the complexes [28]. The $\delta_s(\text{CF}_3)$ mode (symmetric deformation of CF_3) of LiTF located at 777 cm^{-1} and the $\rho(\text{CH}_2)$ mode ($\text{C}-\text{H}_2$ rocking) of MG30 at 750 cm^{-1} (Fig. 3b(i and ii)) are observed to be downshifted and upshifted to 768 and 753 cm^{-1} , respectively, in the presence of 45 wt% LiTF as can be seen in Fig. 3b(iv). The shifting of the $\delta_s(\text{CF}_3)$ band is in good

Fig. 2 ATR-FTIR spectrum of pure MG30 in the wavenumber range from $650\text{--}3250\text{ cm}^{-1}$

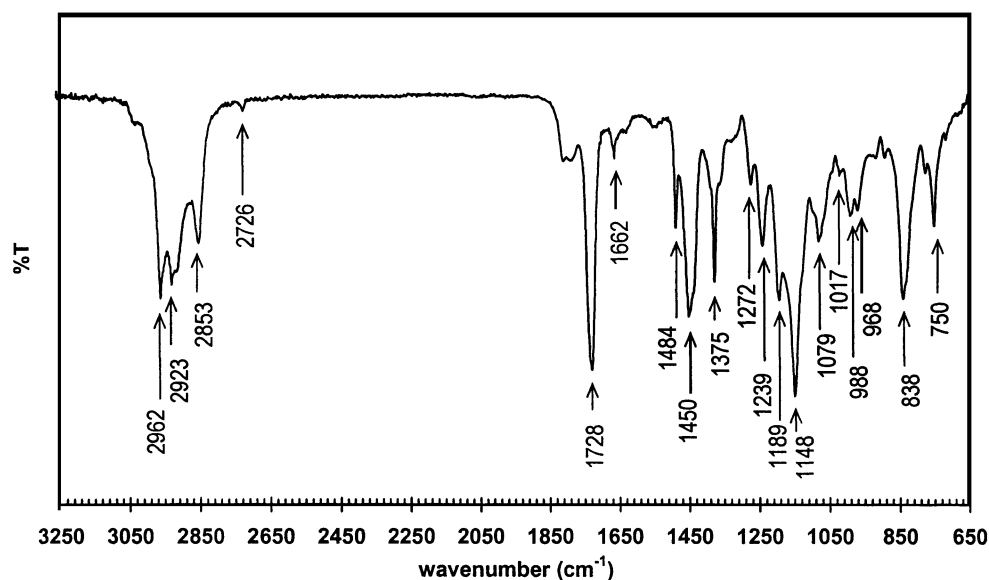


Table 1 MG30 vibrational assignments

Wave number (cm ⁻¹)	Assignment
1,728	C=O symmetric stretching of PMMA
1,662	C=C stretching of Polyisoprene
1,484	CH ₃ asymmetric stretch of PMMA
1,450	O–CH ₃ asymmetric deformation of PMMA
1,375	CH ₃ symmetric deformation of Polyisoprene
1,272	C–O stretching of –COO– of PMMA
1,239	CH ₂ twisting of polyisoprene
1,189	C–H ₂ in plane bending of Polyisoprene
1,148	CH ₂ twisting of PMMA
1,079	CH ₃ rocking of Polyisoprene
1,017	C–C stretching of Polyisoprene
988	C–O–C symmetric of PMMA
968	C–H ₂ out of plane bending of Polyisoprene
838	C(CH ₃) ₂ skeletal vibration of PMMA
750	C–H ₂ rocking of PMMA

agreement with reports by Winie and Arof [29]. Because the $\delta_s(\text{CF}_3)$ of LiTF is highly sensitive to ionic association because of formation of ion pairs and aggregates, the shift of the band from 777 cm⁻¹ to a lower wave number is

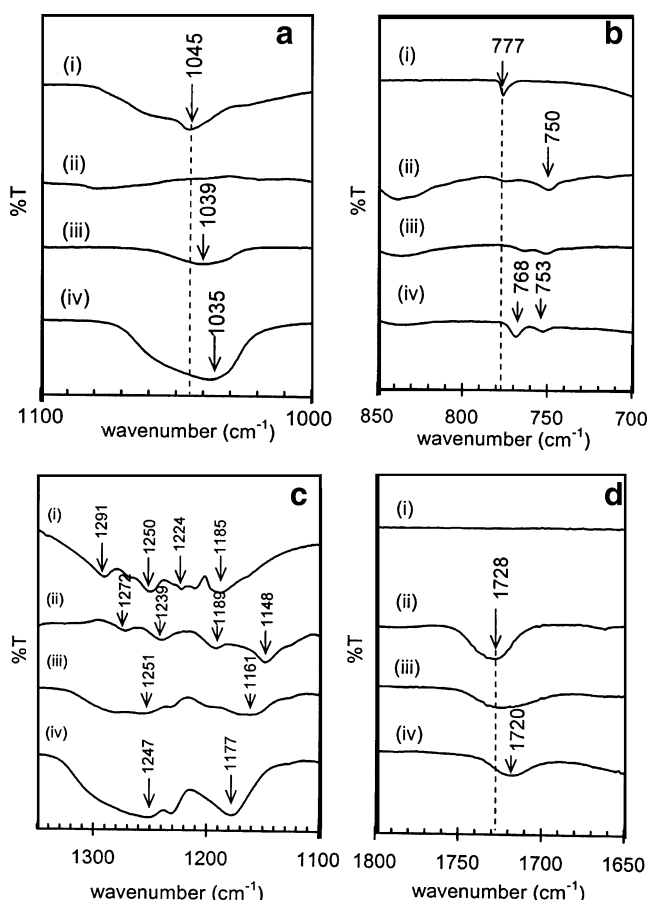


Fig. 3 ATR-FTIR spectra of (i) pure LiTF, (ii) pure MG30, (iii) MG30+35%LiTF and (iv) MG30+45%LiTF in the wave number region of **a** 1,000–1,100, **b** 700–850, **c** 1,100–1,350, and **d** 1,650–1,800 cm⁻¹

highly indicative of the presence of ionic aggregation of $[\text{Li}_2\text{TF}]^+$ species, which has also been observed in other reported works [30]. Such aggregation implies a decrease in the number of free ions from the salt, which could explain the decrease in conductivity of the samples.

In the region of 1,100 to 1,350 cm⁻¹ (Fig. 3c), the $\nu_{\text{as}}(\text{SO}_3)$ mode (asymmetric stretching of SO_3) located at 1,291 and 1250 cm⁻¹, the $\nu_s(\text{CF}_3)$ mode (symmetric stretching of CF_3) at 1,224 cm⁻¹ of the triflate ion, the C–O stretching mode at 1,272 cm⁻¹, and the CH_2 twisting mode at 1,239 cm⁻¹ of the MG30 have merged to form a small shoulder and a broad band centered at 1,251 cm⁻¹ as observed in Fig. 3c(iii). The broad band subsequently shifts to a lower wave number at 1,247 cm⁻¹ as shown in Fig. 3c(iv) as the percentage of LiTF is increased in the mixture. This may be due to the wave numbers of $\nu_{\text{as}}(\text{SO}_3)$ and $\nu_s(\text{CF}_3)$ of the salt and the C–O and CH_2 stretching and twisting modes of MG30 being superimposed on each other. A peak located at 1,185 cm⁻¹ observed in the spectrum of pure LiTF (Fig. 3c(i)) could be assigned to the $\nu_{\text{as}}(\text{CF}_3)$ mode (asymmetric stretching of CF_3). This peak is seen to overlap with the C–H₂ in plane bending mode ($\delta_s(\text{CH}_2)$) at 1,189 cm⁻¹ and also merge with the CH_2 twisting mode ($\tau(\text{CH}_2)$) at 1,148 cm⁻¹ of the MG30 (Fig. 3c(ii)) to form a broad band centered at 1,161 cm⁻¹ with a shoulder at the higher wave number region as observed in Fig. 3c(iii). This band further shifts to 1,177 cm⁻¹ with the full wave half maximum of the band becoming sharper when 45 wt% of LiTF is added (Fig. 3c(iv)). These changes suggest that the environment of the CF_3 vibrational mode has changed as a result of complexation with MG30. Another evidence of polymer–salt interaction can be observed at the C=O stretching mode of MG30. It is found that this carbonyl stretch located at 1,728 cm⁻¹ in the spectrum of pure MG30 is shifted to a lower wave number at 1,720 cm⁻¹ with reduced relative intensity upon incorporation of the lithium salt (Fig. 3d(ii and iv)). This implies a possible complexation between MG30 and LiTF. This observation is consistent with the results reported by Kumutha and Alias [26].

PC–salt interactions

The spectroscopic study was also carried out on the PC–LiTF solution to examine the interactions between LiTF salt and PC plasticizer. Some evidence of the interactions between lithium ion and PC occur in the spectral region of 650 to 2,000 cm⁻¹. In the region of 1,600–2,000 cm⁻¹, the spectra of pure PC shows a strong carbonyl band centered at 1,788 cm⁻¹, which has shifted to 1,775 cm⁻¹ in the spectrum of PC+35 wt% LiTF as shown in Fig. 4a. The shifting of the carbonyl band implies the coordination of $\text{Li}^+ \leftarrow \text{O}=\text{C}$. Similar results have been reported in previous

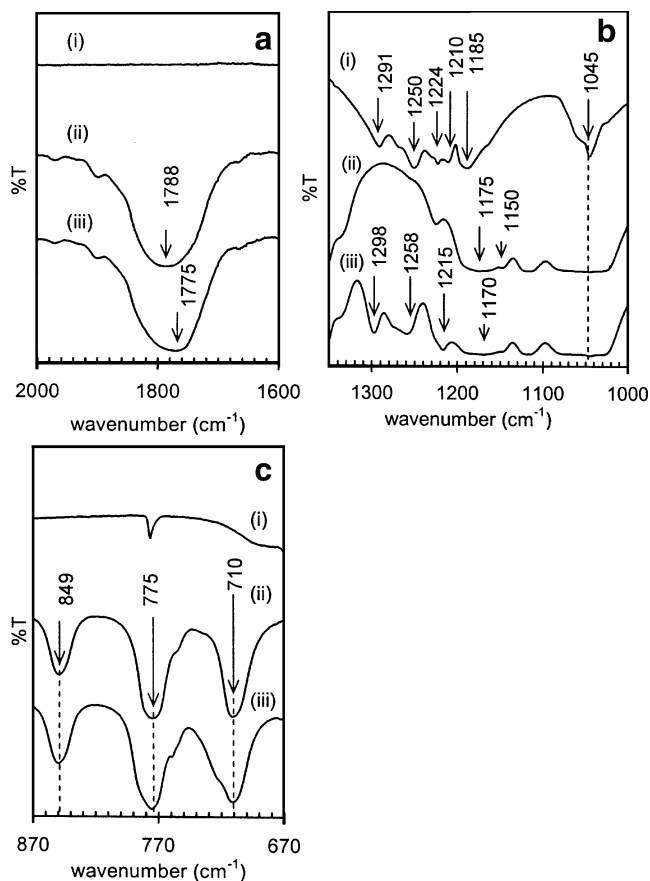


Fig. 4 ATR-FTIR spectra of (i) pure LiTF, (ii) pure PC, and (iii) PC+35% LiTF in the wave number regions of **a** 1,600–2,000, **b** 1,000–1,350, and **c** 670–870 cm^{-1}

works [19, 26, 31]. In the spectral region between 1,000 and 1,350 cm^{-1} , LiTF exhibits an intense peak at 1,185 cm^{-1} , which can be assigned to $\nu_{\text{as}}(\text{CF}_3)$ mode as shown in Fig 4b(i). This band has merged with the band because of $\nu(\text{C-O})+\omega(\text{C-H})$ of PC centered at 1,175 cm^{-1} [19] to form a band centered at 1,170 cm^{-1} with a small shoulder at 1,150 cm^{-1} , which have appeared to be undeviated from its initial position. The disappearance of the $\nu_{\text{s}}(\text{SO}_3)$ mode of LiTF at 1,045 cm^{-1} can also be seen upon addition of PC. This is probably due to this band being buried in the band of PC. The characteristics bands of LiTF at 1,210 and 1,224 cm^{-1} ascribed to $\nu_{\text{s}}(\text{CF}_3)$ mode are observed to merge to form a single band at 1,215 cm^{-1} with increasing intensity upon incorporation of PC. The $\nu_{\text{as}}(\text{SO}_3)$ band located at 1,250 cm^{-1} is broadened and shifted to 1,258 cm^{-1} , and another $\nu_{\text{as}}(\text{SO}_3)$ band located at 1,291 cm^{-1} also undergoes changes in its position and relative intensity to 1,298 cm^{-1} in the PC–LiTF spectrum. The upshift of these bands in the PC–LiTF is suggested to be caused by the interaction of Li^+ ions with the oxygen atom of $\text{O}=\text{C}$ of PC. This behavior is also observed in the DEC–LiTF system [29]. In the region, between 670 and 870 cm^{-1} of the spectrum shown in Fig. 4c, PC exhibits

two intense peaks at 710 cm^{-1} (symmetric ring deformation or breathing mode) and at 775 cm^{-1} (ring deformation or breathing mode), which have broadened with the presence of a small shoulder near the 710 cm^{-1} peak in PC+35 wt% LiTF. The existence of a small shoulder at higher wave number region implies the presence of Li^+ –PC interaction. This observation is similar to those observed in previous reports [19, 23, 32]. The band at 849 cm^{-1} corresponds to the ring stretching–breathing mode of PC. This band showed no appreciable change in its position and shape for the PC–35 wt% LiTF sample. This is consistent with the results reported in reference [19].

Polymer–PC interaction

The effect of plasticizer on the polymer was also studied to note any difference in the behavior of MG30 upon the addition of PC. Infrared spectra of MG30 containing PC with a 1:1 weight ratio concentration in the region between 650 and 1950 cm^{-1} are presented in Fig. 5. For comparison purposes, the spectra of pure MG30 and pure PC are also included. In this region, the CH_3 rocking mode, CH_3 symmetric deformation mode, and CH_2 twisting mode of MG30 can be observed at 1,079, 1,375, and 1,484 cm^{-1} , respectively. In the same spectrum, $\text{C}=\text{C}$ and $\text{C}=\text{O}$ bands located at 1,662 and 1,728 cm^{-1} can also be observed. As can be seen from these spectra, there is no noticeable change in the vibrational frequencies and the band shapes of the MG30–PC system suggesting that there is no interaction between MG30 and PC.

Effect of PC on the polymer–salt interaction

Figure 6 shows the infrared spectra of PC–MG30–LiTF with a composition of 1:1 for PC/MG30. The band at 710, 775, and 849 cm^{-1} as shown in Fig. 6a(ii) because of PC–LiTF interactions as discussed earlier in “ATR-FTIR spectroscopy of pure polymer (MG30)” has reduced greatly

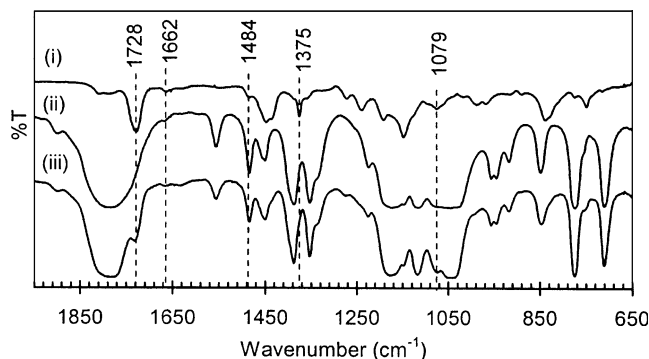


Fig. 5 ATR-FTIR spectra of (i) pure MG30, (ii) pure PC, and (iii) MG30+PC (1:1) in the 650–1,950 cm^{-1} wavelength region

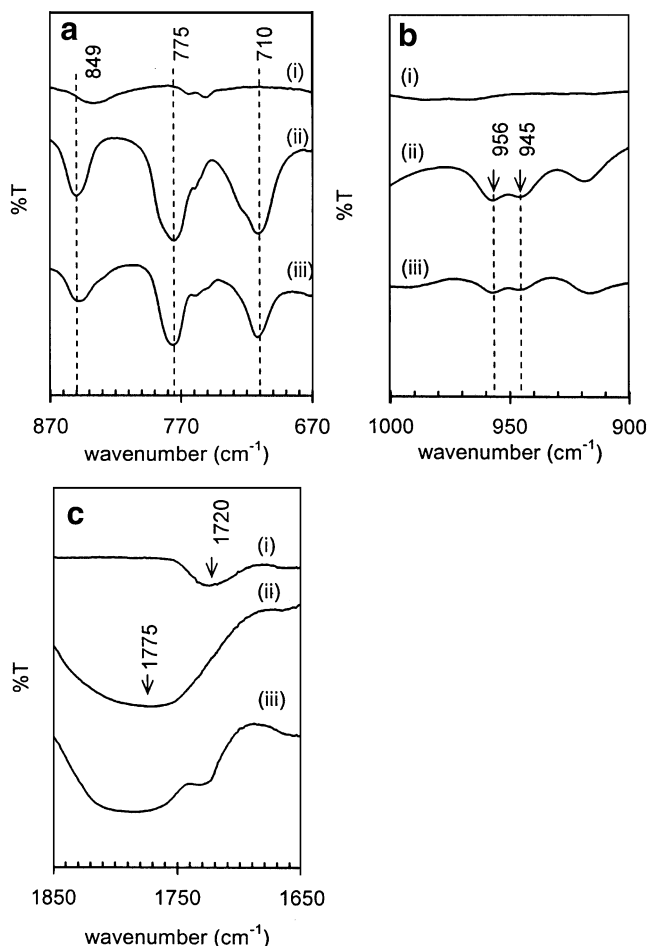


Fig. 6 ATR-FTIR spectra of (i) MG30+35%LiTF, (ii) PC+35%LiTF, and (iii) MG30+PC+35%LiTF in the wavelength region of **a** 670–870, **b** 900–1,000, and **c** 1,650–1,850 cm^{-1}

in intensity in the plasticized samples (Fig. 6a(iii)). The C–O stretching and CH_2 rocking modes of PC [33] remain unshifted at 945 and 956 cm^{-1} , respectively, in the presence of LiTF but reduced in intensity in the presence of MG30 (Fig. 6b(ii) and iii)). These characteristics are due to the greater ionic interaction between MG30 and LiTF compared to the ionic interaction between PC and LiTF. The broad peak in the C=O stretching region of the PC–LiTF interaction (Fig. 6c(ii)) is seen to have narrowed with a shoulder developing at the low frequency region between 1,720 and 1,740 cm^{-1} in the plasticized polymer–salt complexes as represented in Fig 6c(iii). This suggests that there is a competition between the interaction of $\text{Li}^+ \leftarrow \text{O}=\text{C}$ coordination of MG30 with that of $\text{Li}^+ \leftarrow \text{O}=\text{C}$ coordination of PC in the plasticized sample. MG30 being a bigger molecule than PC, the presence of the broad shoulder (1,720–1,740 cm^{-1}) indicates that there is a stronger interaction between MG30–LiTF when compared to PC–LiTF. Hence, it is assumed that the plasticizer PC in the polymer–salt complexes had penetrated into the polymer

matrix to cause an increase in the free volume of the polymer, which in turn enhances its segmental motion. From the changes in the IR spectra, it can be suggested that the interaction between Li^+ and MG30 is stronger than the interaction between Li^+ and PC. The interactions among the components of MG30, PC, and LiTF may help in correlating and discerning the ionic conductivity trend in the MG30 electrolyte system, which is discussed next.

AC impedance studies

Figure 7 shows the AC impedance spectra of various compositions of MG30 gel electrolyte systems for a fixed ratio of MG30 (65)–LiTF (35) at ambient temperature. The Z'' vs Z' plots depict a tilted spike indicating that there is good contact between the electrode and electrolyte. Such plots may be obtained because of the soft physical characteristics of the electrolyte films, and the same behavior was observed for all samples. The experimental data can be fitted well with the equivalent circuit as shown in the inset of Fig. 7 in which R_b is the bulk electrolyte resistance and CPE is a constant phase element. The existence of CPE could be possibly due to a capacitor that changes with frequency and arises if there is air present in between the electrode–electrolyte gap. According to previous reports [34–36], if the complex impedance plot consists of a tilted spike displaced from the origin, the equivalent circuit may be represented by a resistor in series with a CPE. Furthermore, Armstrong [37] reported that the high frequency part of impedance plots can be related to the bulk relaxation process and the low-frequency spur results from

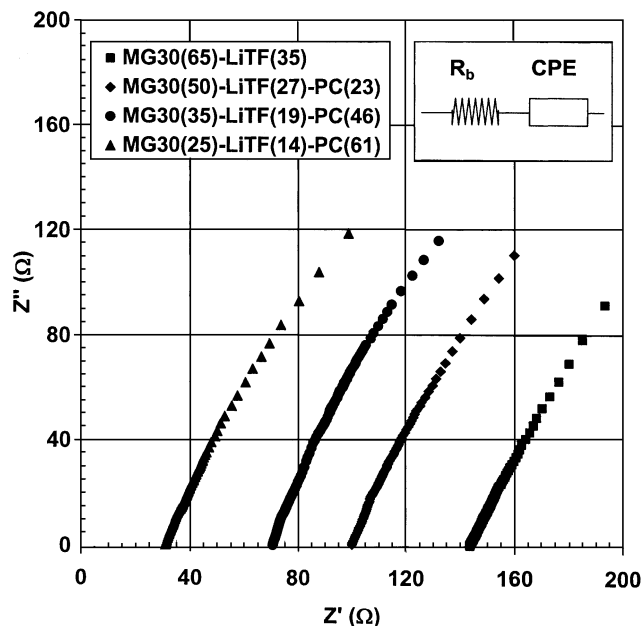


Fig. 7 Representative complex impedance plot of MG30 gel electrolytes at room temperature

electrode–electrolyte interface properties. Thus, the bulk resistance (R_b) was obtained by considering the intercept of the real impedance axis at the high frequency side in the impedance plot and thus gives the total ionic conductivity.

Figure 8 demonstrates the variation of LiTF content vs σ of the MG30–LiTF system. It is found that the conductivity increases as LiTF concentration increases and reaches a maximum value of $8.40 \times 10^{-4} \text{ S cm}^{-1}$ at 35 wt% of LiTF after which the conductivity decreases. The decrease in conductivity observed above 35 wt% of LiTF in MG30–LiTF systems could be explained in terms of a steady decline of free ions because of aggregation. This is supported by ATR-FTIR studies discussed earlier, which shows the presence of bands at 1,045 and 777 cm^{-1} at higher salt concentrations corresponding to the formation of mononate ion pairs forming the aggregate species $[\text{Li}_2\text{TF}]^+$ in the sample. The explanation concerning the increase and decrease in ionic conductivity can be correlated to the phenomenon of ions dissociation and association as reported in many works [38, 39], and the conductivity graph can be divided into three regions. In region a, the introduction of lithium salt, which undergoes ion dissociation because of the presence of C=O in the side chain of MG30, cause a rise in conductivity. It is observed that the slow conductivity increment in this region is proportional to the salt concentration because more Li^+ is dissociated with an increase in salt content. In fact, the initial increase in conductivity is due to the increment in the number of charge carriers. In the region b, further increment in conductivity could be attributed to the increase in the rate of ion dissociation. It can be seen that the highest conductivity is obtained in this region. This is probably due to the effects of the interaction between the charge carriers and the polymer, which influences the segmental

mobility of the polymer chains. During the polymer–salt interaction, Li^+ ions, which juts out at the oxygen atom at the side chain of the carbonyl functional group of the C=O bond, diffuses over the polymer chain as a result of the flexible segmental motion of the chains. This is in good agreement with the explanation offered by Mellander and Albinsson [40] who reported that ion dissociation and polymer segmental motion are the most important aspects in optimizing ionic conductivity in the polymer electrolyte. In region c, the decline in conductivity with a high salt concentration could be due to ion association as mentioned earlier. If this is prominent, it will affect the mean distance between the ions, which become more significant because the ions become closer to one another and they tend to associate. Because the ions are so close to each other, the dissolved Li^+ coordinating to the oxygen in the carbonyl group in MG30 may form a transient crosslink between the chain segments. This could explain the further decrease in segmental flexibility with increasing concentration of salts in region c. Therefore, the film with such salt contents conforming to region c in the present work is not as soft as the low salt content films. These physical properties indirectly indicate that the high salt concentration has caused chain interlinking. Because of this interlinking, the mobility of the charge carriers is greatly reduced leading to a decrease in conductivity. Figure 9 shows how the crosslink may be formed because of the higher salt loading in the polymer chains.

Effect of plasticizers on conductivity

Figure 10 depicts the increment in conductivity values upon addition of plasticizer. From the plot, it is seen that ionic conductivity increases as the content of plasticizer increases. Such increment can be explained by the plasticization/lubrication effect of the plasticizer causing

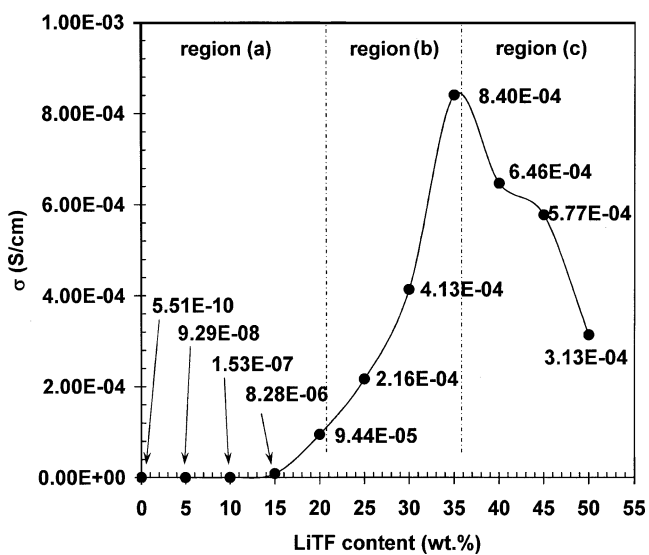


Fig. 8 Ionic conductivity of MG30–LiTF as a function of salt content

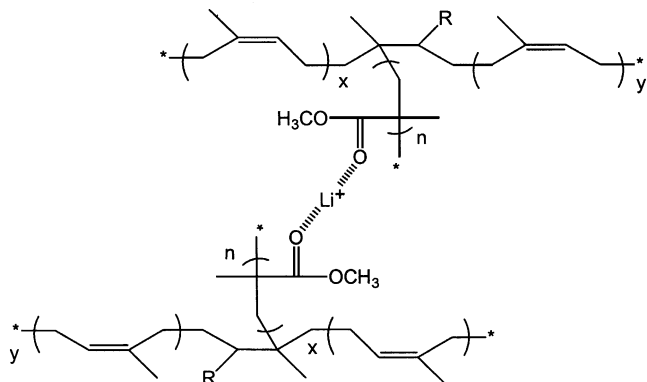


Fig. 9 Formation of transient crosslink via cation. The effect is to reduce segmental mobility and decrease the overall ion mobility (in the structure: R is a free radical)

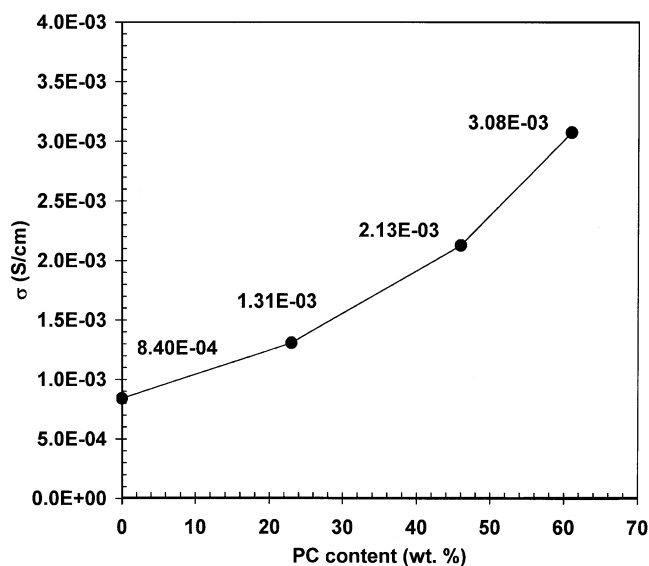


Fig. 10 Ionic conductivity vs plasticizer content of MG30 (65)–LiTF (35) at room temperature

an increase in the flexibility of the host polymer, which leads to an increase in conductivity value, which is consistent with the finding by Yahya and Arof [18]. This is supported by the evidence provided in ATR-FTIR studies discussed in the previous section where the broad shoulder at $1,720\text{--}1,740\text{ cm}^{-1}$ because of the MG30–LiTF interaction is also present in the MG30–LiTF-plasticized system. The effect of segmental flexibility is responsible for the formation of free volume, which enhances the ionic conductivity of the plasticized system. This phenomenon is much pronounced in the literature [16], and the free volumes are considered to exist above T_g . From ATR-FTIR studies, it was observed that the band at $1,045\text{ cm}^{-1}$ attributed to $\nu_{\text{as}}(\text{SO}_3)$ gets buried in the spectra of PC+LiTF indicating that PC does not cause LiTF to dissociate. The role it plays is therefore to provide lubricating effects as evidenced from ATR-FTIR studies in “Effect of PC on the polymer–salt interaction” where it is observed that there is a weak interaction between PC and LiTF but greater interaction between MG30 and LiTF. However, the addition of more plasticizer results in a decrease in the mechanical stability of the sample, and hence an optimum plasticizer concentration is reached. In this case, it is observed that the PC content of up to 61 wt% exhibits the highest ionic conductivity as well as sustaining the freestanding film form. Above this composition, the gel film becomes mechanically unstable. The rise in conductivity during incorporation of plasticizer is in good agreement with previous reports [41–42]. Jaipal Reddy et al. [43] and Subba Reddy et al. [44] reported that the inclusion of plasticizer induce greater flexibility in the polymer host, which can be correlated to the reduction in T_g as shown in Table 2. The plasticizer also causes an increase in the local

Table 2 Activation energy and glass transition (T_g) values of MG30 gel electrolytes

Composition MG30/LiTF/PC	T_g (°C)	Regression value, R^2	Activation energy, E_a (eV)
65/35/0	−66.61	0.997	0.163
50/27/23	−69.19	0.997	0.160
35/19/46	−70.40	0.999	0.146
25/14/61	−74.60	0.997	0.144

viscosity of the polymer chains, which in turn acts on ion pairs to promote more dissociation of ions consequently boosting up the carrier concentration. This is manifested in the high conductivity value at that concentration of plasticizer. Therefore, the plasticizer can be said to act just as a lubricant in this system where the lubricating action is manifested as a rise in conductivity of the system. Because the effect between the plasticizer and the polymer–salt electrolyte has crucial significance on the conductivity of the plasticized system, it is suggested that the plasticizer favors the polymer–cation interaction by inducing Li^+ to make a pseudointeraction with the plasticizer, which in turn increases the ionic conductivity. Furthermore, the effect of higher dielectric constant (ϵ) of the plasticizer is also significant, and PC with $\epsilon=66.14$ causes isolation of the Li^+ cation by surrounding it in the polymer chains, which results in the lowering of the transient cross-linking of the polymer host, thereby increasing the free volume. The plasticizer also perturbs the polymer–polymer interchain crosslink by increasing inter- and intrachain separation and hence increases the free volume of the system further. The decrease in polymer–polymer interchain crosslink effectively influences the T_g value, which is seen to reduce in the plasticized samples as shown in Table 2. Consequently, the plasticizer amplifies the polymer segmental motion, which

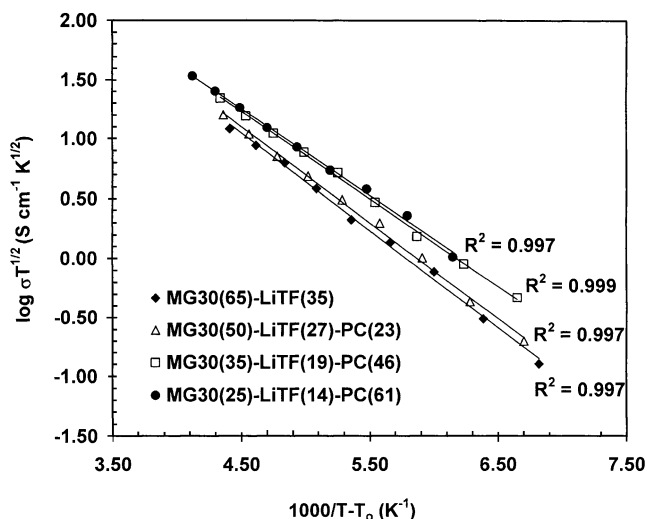


Fig. 11 VTF plot of plasticized and unplasticized MG30 gel electrolytes at the highest conductivity composition of MG30–LiTF salt systems

facilitates the ionic mobility resulting in higher conductivities. This behavior is in good agreement with Gray [45] who reported that the lithium ion may prefer to conduct through the plasticizer rich phase because of the medium being less viscous and hence enhancing the mobility of the ions. Therefore, the plasticized electrolyte films exhibit an enhancement in conductivity when compared to the unplasticized system.

Temperature dependence conductivity

Figure 11 demonstrates the Vogel–Tamman–Fulcher (VTF) plot of plasticized and unplasticized MG30–LiTF electrolyte based on the equation below:

$$\sigma(T) = AT^{-1/2} \exp \frac{-B}{k(T - T_0)}$$

where T is the absolute temperature and A , B , and T_0 are fitting constants. A is a constant that is proportional to the number of charge carriers, B maybe considered as a pseudoactivation energy, k is the Boltzmann constant, and T_0 is the critical temperature at which the free volume disappears and the configurational entropy becomes zero, usually 30–50° below T_g [46]. The T_g of each sample was obtained by differential scanning calorimetry scan, and the results are tabulated in Table 2. It is observed that ionic conductivity increases linearly with the increase in temperature. The regression values, R^2 , of both systems MG30–LiTF and MG30–LiTF–PC lies in the range of 0.997 and 0.999 indicating that the plots are straight line graphs. This shows that the conductivity conforms to obey the VTF behavior. The activation energy (E_a) of MG30-based electrolytes was calculated by obtaining the gradient of the slope of the $\log \sigma T^{1/2}$ vs $1,000/T - T_0$ as shown in Table 2. It can be seen that the activation energy decreases as the weight percent of plasticizer increases with the E_a value of the unplasticized system being around 0.163 eV. This value decreases to about 12% upon incorporation of the plasticizer up to 61 wt% concentration. The decrease in E_a with the PC content is a reflection of the enhancement in polymer host segmental motion. These results agree with the results obtained by impedance spectroscopy, which show that conductivity increases with the increase in plasticizer content up to 61 wt%. The reduction in E_a as the concentration of plasticizer increase may be explained in terms of the free volume concept. When temperature is increased, the vibrational energy of a segment is sufficient to push against the hydrostatic pressure imposed by its neighboring atoms and create a small amount of space surrounding its own volume in which vibrational motion can occur. The free volume existing around the polymer chain favors the mobility of ions and hence conductivity. This feature promotes the movement of ions through the

plasticizer-rich phase, and the conducting activity will take place via the viscous matrix.

Conclusion

The ATR-FTIR analysis manifested the interactions among the various components of system namely, the plasticizer, salt, and polymer as frequency changes in the internal vibrational mode. The complexation between MG30–LiTF and PC–LiTF is evaluated by observing the changes in position, shape, and intensity of C=O peaks. It is established that the $\text{Li}^+ \leftarrow \text{O}=\text{C}$ interaction of the carbonyl functional group of MG30 is stronger than the carbonyl group of PC. There is no interaction between MG30 and PC as there are no significant changes in the vibrational modes and shape of relevant bands of functional group such as the C=O, C–C, CH_3 , and CH_2 studied. The conductivity of MG30–LiTF electrolytes increases with increasing concentration of LiTF up to 35 wt % and then decreases at higher LiTF concentration because of ion aggregation. The highest conductivity obtained is in the order of $10^{-4} \text{ S cm}^{-1}$, and this value is improved by one order of magnitude upon addition of PC at room temperature for all compositions studied. PC causes greater segmental motion by penetrating the polymer matrix. The increase in conductivity could be correlated to the decrease in the E_a value. The temperature-dependent conductivity behavior confirms that the ionic conductivity behavior follows the VTF rule and justifies the suggestion that all samples are amorphous in the temperature range of study.

Acknowledgment The authors would like to thank the government of Malaysia for the IRPA grant no. 09-02-01-0068EA0068.

References

1. Fenton DE, Parker JM, Wright PV (1973) *Polymer* 14(11):589
2. Armand MB, Chabagno JM, Duclot M (1978) In: Ext. Abstr. Second International Meeting on Solid Electrolytes, St. Andrews, Scotland
3. Armand MB, Chabagno JM, Duclot M (1979) In: Vashista P, Mundy JN, Shenoy GK (eds) *Fast ion transport in solids*. Elsevier, Amsterdam
4. Dissanayake MAKL, Careem MA (1988) *Solid State Ionics* 28–30:1093–1097
5. Su L, Xiao Z, Lu Z (1998) *Mater Chem Phys* 52(2):180–183
6. Periasamy P, Tatsumib K, Shikanob M, Fujiedab T, Sakaib T, Saitob Y, Mizuhata M, Kajinami A, Deki S (1999) *Solid State Ionics* 126(3–4):285–292
7. Dafader NC, Haque ME, Akhtar F, Ahmad MU (2006) *Radiat Phys Chem* 75(1):168–172
8. Jarvis CR, Macklin WJ, Macklin AJ, Mattingley NJ, Kronfli E (2001) *J Power Sources* 97–98:664–666
9. Adebahr J, Gavelin P, Jannasch P, Ostrovskii D, Wesslen B, Jacobsson P (2001) *Solid State Ionics* 135(1–4):149–154
10. Nasef MM, Saidi H (2006) *Mater Chem Phys* 99(2–3):361–369

11. Idris R, Glasse MD, Latham RJ, Linford RG, Schlindwein WS (2001) *J Power Sources* 94(2):206–211
12. Glasse MD, Idris R, Latham RJ, Linford RG, Schlindwein WS (2002) *Solid State Ionics* 147(3–4):289–294
13. Bishop AG, MacFarlane DR, McNaughton D, Forsyth M (1996) *Solid State Ionics* 85(1–4):129–135
14. Cheradame H, LeNest JF (1987) In: MacCallum JR, Vincent CA (eds) *Polymer electrolyte reviews—1*. Elsevier, London
15. Furlani M, Kalinga Bandara LRA, Mellander BE (1997) *Electrochim Acta* 43(10–11):1517–1523
16. Gray FM (1997) *Polymer electrolytes*. The Royal Society Chemistry, London
17. Southall JP, Hubbard HVStA, Johnston SF, Rogers V, Davies GR, McIntyre JE, Ward IM (1996) *Solid State Ionics* 85(1–4):51–60
18. Yahya MZA, Arof AK (2003) *Eur Polym J* 39(5):897–902
19. Deepa M, Sharma N, Agnihotry SA, Chandra R (2002) *J Mater Sci* 37(9):1759–1765
20. Rajendran S, Sivakumar M, Subadevi R (2004) *Mater Lett* 58(5):641–649
21. Jacob MME, Arof AK (2000) *Electrochim Acta* 45(10):1701–1706
22. MacFarlane DR, Meakin P, Bishop A, McNaughton D, Rosali JM, Forsyth M (1995) *Electrochim Acta* 40(13–14):2333–2337
23. Frech R, Chintapalli S (1996) *Solid State Ionics* 85(1–4):61–66
24. Chintapalli S, Frech R (1996) *Solid State Ionics* 86–88:341–246
25. Pavia DL, Lampman GM, Kriz GS (1996) *Introduction to spectroscopy*. Saunders College, USA
26. Kumutha K, Alias Y (2006) *Spectrochim Acta Part A* 64(2):442–447
27. Arjunan V, Subramanian S, Mohan S (2001) *Spectrochim Acta Part A* 57(13):2547–2554
28. Subban RHY, Arof AK (2004) *Eur Polym J* 40(8):1841–1847
29. Winie T, Arof AK (2006) *Spectrochim Acta Part A* 63:677–684
30. Starkey SR, Frech R (1997) *Electrochim Acta* 42(3):471–474
31. Deepa M, Agnihotry SA, Gupta D, Chandra R (2004) *Electrochim Acta* 49(3):373–383
32. Battisti D, Nazri GA, Klassen B, Aroca R (1993) *J Phys Chem* 97(22):5826–5830
33. Stephan AM, Kumar TP, Renganathan NG, Pitchumani S, Thirunakaran R, Muniyandi N (2000) *J Power Sources* 89(1):80–87
34. Lee WJ, Jung HR, Lee MS, Kim JH, Yang KS (2003) *Solid State Ionics* 164:65–72
35. Kim HS, Shin JH, Moona SI, Kim SP (2003) *Electrochim Acta* 48:1573–1578
36. Vondrak J, Reiter J, Velicka J, Klapste B, Sedlarikova M, Dvorak J (2005) *J Power Sources* 146:436–440
37. Armstrong RD (1974) *J Electroanal Chem* 52:413–419
38. Osman Z, Ibrahim ZA, Arof AK (2001) *Carbohydr Polym* 44:167–173
39. Ferloni P, Mastragostino M, Menenghello I (1996) *Electrochim Acta* 41:27–33
40. Mellander BE, Albinsson I (1996) In: Chowdari BVR, Dissanayake MAKL, Carrem MA (eds) *Solid state ionics: new developments*. World Scientific, Singapore
41. Yang XQ, Lee HS, Hanson L, McBreen J, Okamoto Y (1995) *J Power Sources* 54:198–204
42. Andrieu X, Vicedo T, Fringant C (1995) *J Power Sources* 54:487–490
43. Jaipal Reddy M, Sreekanth T, Subba Rao UV (1999) *Solid State Ionics* 126:55–63
44. Subba Reddy ChV, Sharma AK, Narasimha Rao VVR (2002) *J Power Sources* 111:357–360
45. Gray FM (1991) *Solid polymer electrolytes: fundamental and technological applications*. Wiley, New York
46. Ratner MA (1987) In: MacCallum JR, Vincent CA (eds) *Polymer electrolyte reviews—1*. Elsevier, London